



**HAL**  
open science

## Studies and optimization of scintillation light measurements for the development of the 3-gamma medical imaging XEMIS2 liquid xenon Compton camera

Yuwei Zhu, S. Acounis, N. Beaupère, J.L. Beney, J. Bert, S. Bouvier, D. Cai, C. Canot, T. Carlier, M. Cherel, et al.

### ► To cite this version:

Yuwei Zhu, S. Acounis, N. Beaupère, J.L. Beney, J. Bert, et al.. Studies and optimization of scintillation light measurements for the development of the 3-gamma medical imaging XEMIS2 liquid xenon Compton camera. Nuclear Instruments and Methods in Physics Research Section A: Accelerators, Spectrometers, Detectors and Associated Equipment, 2023, 1047, pp.167794. 10.1016/j.nima.2022.167794 . hal-03891903

**HAL Id: hal-03891903**

**<https://hal.science/hal-03891903v1>**

Submitted on 17 Mar 2023

**HAL** is a multi-disciplinary open access archive for the deposit and dissemination of scientific research documents, whether they are published or not. The documents may come from teaching and research institutions in France or abroad, or from public or private research centers.

L'archive ouverte pluridisciplinaire **HAL**, est destinée au dépôt et à la diffusion de documents scientifiques de niveau recherche, publiés ou non, émanant des établissements d'enseignement et de recherche français ou étrangers, des laboratoires publics ou privés.

Copyright



## Studies and optimization of scintillation light measurements for the development of the 3-gamma medical imaging XEMIS2 liquid xenon Compton camera

Y. Zhu<sup>a,1,\*</sup>, S. Acounis<sup>a</sup>, N. Beaupère<sup>a</sup>, J.L. Beney<sup>a</sup>, J. Bert<sup>b</sup>, S. Bouvier<sup>a</sup>, D. Cai<sup>a</sup>, C. Canot<sup>a</sup>, T. Carlier<sup>c</sup>, M. Cherel<sup>d</sup>, J.P. Cussonneau<sup>a</sup>, S. Diglio<sup>a</sup>, D. Giovagnoli<sup>b</sup>, J. Idier<sup>e</sup>, F. Kraeber-Bodéré<sup>c</sup>, P. Le Ray<sup>a</sup>, F. Lefèvre<sup>a</sup>, J. Masbou<sup>a</sup>, E. Morteau<sup>a</sup>, J.S. Stutzmann<sup>a</sup>, D. Visvikis<sup>b</sup>, Y. Xing<sup>a</sup>, D. Thers<sup>a</sup>

<sup>a</sup> SUBATECH, IMT Atlantique, CNRS/IN2P3, Université de Nantes, 44307 Nantes, France

<sup>b</sup> INSERM, UMR1101, LaTIM, CHRU Morvan, 2 avenue Foch, Brest, 29600, France

<sup>c</sup> Centre Hospitalier Universitaire de Nantes, 1 place Alexis-Ricordeau, 44093 Nantes, France

<sup>d</sup> INSERM U1232 équipe 13, 8 quai Moncousu, 44000 Nantes, France

<sup>e</sup> LS2N, Ecole Centrale de Nantes, CNRS/IN2P3, Université de Nantes, 44307 Nantes, France

### ARTICLE INFO

#### Keywords:

Liquid xenon  
Compton camera  
Scintillation light  
Medical imaging  
3-gamma imaging  
Time projection chamber

### ABSTRACT

We report the studies and optimization of scintillation light measurements in an updated version of the XEMIS1 prototype for the development of the XEMIS2 camera. A novel monolithic liquid xenon Compton camera, named XEMIS2 (XENon Medical Imaging System), attempts to achieve low-activity small-animal imaging using the 3-gamma imaging technique. This emerging detector relies on the time projection chamber technique: it will be able to perform a simultaneous detection of the three  $\gamma$ -rays emitted by a specific radionuclide, such as scandium-44, and to produce a good quality image with a remarkable diminution of radiopharmaceutical activity at the same time. Vacuum Ultraviolet (VUV) scintillation light and ionization charge carriers generated from the recoiling particles within the detector are detected and used to reconstruct the interaction position and deposited energy. A cost-effective self-triggering scintillation signal read-out and data acquisition (DAQ) system has been developed to achieve a continuous data read-out with negligible electronics dead time. The DAQ prototype has been installed and qualified in an updated version of the XEMIS1 detector. It reaches the performance specifications in scintillation light measurements. Moreover, scintillation signals can also be used for the virtual segmentation of the monolithic detection volume through the matching algorithm of the scintillation and ionization signals based on the Light Collection Map (LCM). This spatial pre-localization of the physical events, called the virtual fiducialization of the active volume, is used to lower the detector occupancy rate when the administered activity is increased to lessen the examination time. The XEMIS1 experimental LCMs indicate that each PMT owns an individual field of view so as to segment the active volume virtually. The preparation work for the XEMIS2 camera operation has been completed in the updated XEMIS1 detector while the XEMIS2 scintillation light measurement system is under commissioning in Nantes Centre Hospitalier Universitaire.

### 1. Introduction

Nuclear medical imaging involves the imaging of radiation emitted by radiopharmaceuticals administered for diagnostic, therapeutic, or research purposes. In the last decades, nuclear medical imaging has brought remarkable enhancement in tumor diagnosis, therapeutic monitoring, and pharmacological development. Three crucial indicators to lead the later advance in nuclear medicine imaging are: the

personalized medicine with more targeted and effective treatments, the reduction of the examination time, and the diminution of the radiopharmaceutical dose, especially for vulnerable patients (e.g., children and pregnant women).

In oncology diagnosis, the 3-gamma imaging developed at the SUBATECH laboratory is an emerging low-activity functional imaging modality that maintains an acceptable image quality with a remarkable diminution of radiotracer activity in comparison with the conventional

\* Corresponding author.

E-mail address: [yuwei.zhu@ijclab.in2p3.fr](mailto:yuwei.zhu@ijclab.in2p3.fr) (Y. Zhu).

<sup>1</sup> Now at IJCLab, Bât. 100, 15 rue Georges Clémenceau, 91405 Orsay, France.

medical imaging techniques [1]. This imaging modality encompasses a kernel notion: the employment of a large Field Of View (FOV) cylindrical Liquid Xenon (LXe) Compton camera to directly reconstruct the three-dimensional (3D) distribution of the radiotracer, labeled with a ( $\beta^+$ ,  $\gamma$ ) radionuclide, for example, the scandium-44 ( $^{44}\text{Sc}$ ) at a comparatively low count rate. The novel radiolabeled compounds using DOTAT-peptides labeled with  $^{44}\text{Sc}$  are under research at SUBATECH laboratory, ARRONAX GIP, CRCI2NA, and Nantes Centre Hospitalier Universitaire (CHU) [2].

The labeled radionuclide (e.g.,  $^{44}\text{Sc}$ ) emits a positron and a third photon almost at the same instant. The annihilation of the positron with an electron produces two back-to-back 511 keV photons, which will be simultaneously detected in the active region of a highly sensitive Compton camera, and then form a Line Of Response (LOR) as in the common Positron Emission Tomography (PET) imaging system. The interaction of the third photon, with an energy of 1.157 MeV, in the Compton camera leads to the reconstruction of a Compton cone with aperture angle  $\theta$  and axis  $\Delta$  through the kinematics of the Compton scattering process. The 3-gamma event can then be directly reconstructed by intersecting the LOR and the Compton cone in the FOV of the camera.

Intending to exploit the experimental feasibility of the 3-gamma imaging modality, the associated camera needs to fulfill some requirements. The reconstruction of the Compton scattering sequence necessitates a good energy resolution and a high spatial resolution of the detector. The distinction between the Compton multi-scattering and the photoelectric single-scattering requires a high detection sensitivity and efficiency of the camera. Besides, the associated detector needs to be capable of measuring the energy, position, and arrival time of the  $\gamma$ -rays with energy around 1 MeV, which can undergo a single or multiple Compton scattering followed by a photoelectric interaction. The LXe Time Projection Chamber (LXeTPC) technique is an appropriate prospect to fulfill the above requirements, which allows for the construction of the specially developed large FOV Compton camera without parallax effect for nuclear medical imaging applications.

Intending to demonstrate the feasibility of low-activity 3-gamma imaging using the LXeTPC technique, we propose and implement an emerging R&D project named XEMIS (XENon Medical Imaging System), based on a LXe Compton camera technology. The 3-gamma imaging combined with the LXeTPC technology is capable of reconstructing, event-by-event, the position of the ( $\beta^+$ ,  $\gamma$ ) emitter from each LOR-cone intersection. Compared with the classical PET reconstruction algorithms, the 3-gamma imaging reconstruction algorithm using the cone-LOR intersection criterion constricts the location of the annihilation point on the LOR [3]. The average 33-mm uncertainty along the LOR obtained from a preliminary full GATE/Geant4 simulation represents a significantly higher resolution than conventional PET imaging [3].

The first small-scale prototype, named XEMIS1, has been carried out and presented promising performances of LXeTPC with a sub-millimeter spatial resolution and an energy resolution of 9% (FWHM) for 511 keV photons under an electric field of 1 kV/cm [4,5]. The second larger dimension prototype, named XEMIS2, is a cylindrical monolithic LXe Compton camera oriented to the 3-gamma small-animal imaging. The long-term objective of the XEMIS project attempts to achieve whole-body imaging or hadrontherapy monitoring for the human body using a sizeable axial FOV LXe Compton camera called XEMIS-HD, which is presently under design.

## 2. XEMIS2 camera

The XEMIS2 detector (enclosed in an elevated low-pressure cryostat) is a monolithic 24 cm axial FOV LXe Compton camera carrying around 200 kg LXe with an ultra-high purity level. The camera contains two identical cylindrical LXeTPCs using a shared central cathode. The detection volume of each single-phase LXeTPC is 12 cm of drift length, 7 cm and 19 cm of inner and outer radius respectively. The LXeTPC

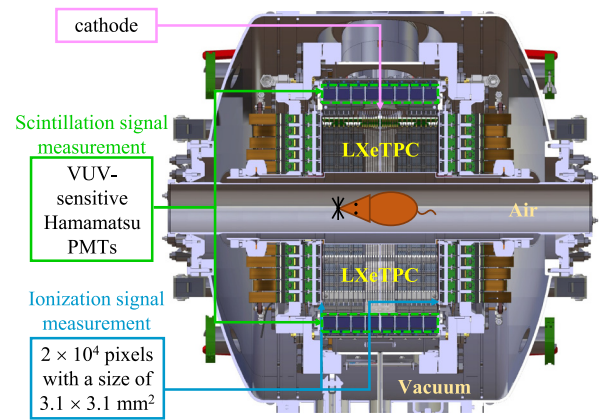


Fig. 1. Longitudinal view of the mechanical design of the XEMIS2 camera.

has a homogeneous active zone with high position sensitivity, which allows for the enhancement of the detection efficiency for the Compton multi-scattering events. Besides, the large axial FOV detector geometry, with a geometrical acceptance for small animals larger than 50% (up to 75% at the center of the FOV), promotes the coincident three  $\gamma$ -rays detection. The longitudinal view of the mechanical design of the XEMIS2 camera is illustrated in Fig. 1.

Vacuum Ultraviolet (VUV) scintillation light and ionization charge carriers generated from the recoiling particles are measured. The scintillation photons are collected by the VUV-sensitive photomultiplier tube (PMT), while the charge carriers created from the ionizing radiations are drifted by a uniform electric field of 2 kV/cm and then collected by two symmetrical pixelated anodes situated at both ends, shielded by the Frisch grids. This drift field is produced by the high voltage of the cathode, and the decreasing voltage of the internal and external field rings set up to the ground on the anode. Each anode employs nearly 10 000 pixels with dimensions of  $3.1 \times 3.1 \text{ mm}^2$ . The induced current signals are then read out and processed by the ultra-low noise electronics with the lowest self-triggering charge threshold level to extract the arrival time of the ionization signal on the anode, transverse (X, Y) coordinates, and deposited energy per interaction point (or interaction vertex) [6,7]. The longitudinal position along the drift direction (Z coordinate) can be deduced from the electron drift time, that is the delay time between the scintillation signal and ionization signal. The  $\gamma$ -ray identification is possible by using the deposited energy and the spatial position per interaction vertex.

With the aim of securely managing almost 200 kg of LXe in a hospital center and keeping the operating conditions inside the XEMIS2 detector cryostat (168 K at 1.2 bar of absolute pressure and ultra-low impurity level below 1 ppb  $\text{O}_2$  equivalent) during long periods of data acquisition, a dedicated closed-loop cryogenic infrastructure, including the high-pressure resistant Recovery Storage system of Xenon (noted as ReStoX) and the xenon purification and recirculation subsystems equipped with the rare-gas purifier getters, are united into the XEMIS2 camera. The complete facility of the XEMIS2 system is illustrated in Fig. 2.

In case of a critical situation (e.g., the loss of cold resources resulting from power supply failure or the detector damage due to the sudden rise of the detector pressure), the total LXe stored in the XEMIS2 detector cryostat can be automatically transferred to the ReStoX tank within 10 min at a mass flow rate of about 1 ton/h using a gravity-assisted method without human intervention [8,9].

## 3. Scintillation light measurement

The difficulty in measuring the scintillation light in XEMIS2 is the measurement of the few scintillation VUV photons generated in the LXeTPCs. As a result of applying a high-intensity electric field of 2 kV/cm,



Fig. 2. Overview of the XEMIS2 facility in Nantes Centre Hospitalier Universitaire (CHU).

to reduce the electron-ion recombination process and to promote the ionization charge collection for  $\gamma$ -rays with energy greater than 100 keV, the scintillation light yield lessens to less than 50% compared to the zero electric field situation [10] (about 46 300 photons/MeV for 1 MeV relativistic electron) because the electron-ion recombination process is suppressed by the high-intensity electric field. As the XEMIS2 camera is a monolithic LXe-based detector, the VUV scintillation light at 178 nm wavelength is emitted isotropically in  $4\pi$  solid angle coverage and then propagates in LXe. Through light reflection or diffusion, some detector components, such as the field rings situated around the active volume, may block the scintillation light propagation to the PMTs. Even though the XEMIS2 camera does not attempt to operate as a LXe-based scintillation electromagnetic calorimeter, the scintillation light collection has been optimized without influencing the ionization charge collection to extract the time information of the 3-gamma event. To achieve a small-animal 3-gamma imaging with 20 kBq activity in 20 min, the active zone is peripherally equipped with 64 VUV-sensitive PMTs immersed in the LXe to detect the emitted VUV photons.

The primary use of the scintillation light in XEMIS2 is to provide the  $\gamma$ -ray interaction time for drift distance calculation. When an electric field of 2 kV/cm is applied in the LXeTPC, the scintillation light is emitted from the decay of a singlet excited state (3%), the decay of a triplet excited state (60%), and the electron-ion recombination process (37%), with decay times of 2.2 ns [11], 27 ns [11], and 45 ns [12] respectively, thus the scintillation light produced by LXe is appropriate for timing applications. Besides, the intrinsic contribution of scintillation light production in LXe for time measurement is associated with the scintillation mechanism in LXe. The intrinsic time resolution improves with the number of detected photoelectrons (p.e.s). For one photoelectron (p.e.) detection, the intrinsic time resolution of LXe is about 36 ns. In contrast, the intrinsic time resolution is around 360 ps when 10 000 p.e.s are detected. For a few p.e.s collection, namely an average of 2 p.e.s per PMT in XEMIS2 for one disintegration of  $^{44}\text{Sc}$ , with two emitted  $\gamma$ -rays of 511 keV and a third  $\gamma$ -ray of 1157 keV, according to the simulations, the intrinsic time resolution of LXe is expected to be the dominant contribution to the time resolution of the scintillation light measurement of each PMT.

Moreover, the scintillation signals can be used for the virtual segmentation of the active zone through the matching algorithm of the scintillation and ionization signals based on the light collection map. When enlarging the administered activity to shorten the examination time, with complete coverage of 368 PMTs, the spatial pre-localization of the physical events is used for lowering the LXeTPC occupancy rate as a result of the non-negligible drift time of the ionization charge up to 52  $\mu\text{s}$ .

A modified geometric configuration operating under an electric field of 2 kV/cm, according to the XEMIS2 design, was used in the XEMIS1

detector to validate the geometry of the field rings configuration and the PMT light collection in XEMIS2. The updated version of the XEMIS1 detector has an active volume of 2.5 cm  $\times$  2.5 cm  $\times$  6.51 cm.

### 3.1. Scintillation signal read-out and data acquisition system

A cost-effective high-rate self-triggering scintillation signal read-out and data acquisition (DAQ) system has been developed, as well as the ionization signal high capability DAQ system, to archive a continuous data read-out with negligible electronics dead time [13]. These two independent DAQ systems are synchronized. The light measurement system is dedicated to extracting the  $\gamma$ -ray interaction time and the approximate number of detected p.e.s from the scintillation signals, which contains three functional units: the Hamamatsu R7600-06MOD-ASSY PMT dedicated for VUV scintillation light detection in LXe [13], the self-developed scintillation signal front-end read-out electronics noted as XSRETOT (XEMIS Scintillation Read-out for Extraction of Time Over Threshold), and the XEMIS Data Concentrator (XDC). The XSRETOT Printed Circuit Board (PCB) contains 16-channel electronic circuits to carry out the signal self-triggering function with a single p.e. sensibility threshold. Each circuit is equipped with a sixth-order low-pass RLC Pulse-Shaping Amplifier (PSA) to integrate shape and amplify the analog pulses delivered by the PMT and a Leading Edge Timing Discrimination (LETD) module. Each PMT channel is self-triggered through the LETD module with a given threshold voltage applied to the shaped pulse. The scintillation signal DAQ system is triggered when the amplitude of the analog pulses, delivered by the PSA, is greater than the applied threshold so the analog shaped pulse can be converted into the Time Over Threshold (TOT) signal by the discriminator. Finally, the corresponding digital data of the affected PMT address, leading edge and trailing edge of the over-threshold shaped pulse from each channel are read out by the Field-Programmable Gate Array (FPGA) of the XDC via the high-speed LVDS (Low Voltage Differential Signaling) cable to accomplish the preliminary online data processing.

For the scintillation signal timing measurement, an optimized LETD method [14] with time walk correction is used to extract the  $\gamma$ -ray interaction time during offline data processing. Besides, since the precise deposited energy is not extracted from the scintillation signals, the approximate number of p.e.s collected by the PMT is given by the TOT technique, which also satisfies the low-cost requirement.

During the offline data processing, the over-threshold shaped scintillation signals from all the PMT channels are sorted by corrected times in chronological order. The signals from the same  $\gamma$ -ray interaction are aggregated in the same cluster with a time window of clusterization of about 100 ns. In the case that a  $\gamma$ -ray undergoes a single or multiple Compton scattering followed by a photoelectric interaction, an overall  $\gamma$ -ray interaction time can be measured for these interaction vertexes. For 3-gamma emission, even if two  $\gamma$ -rays from the same disintegration interact with LXe outside the FOV of the PMTs, their interaction time can be directly given by the interaction time of the remaining  $\gamma$ -ray detected by any PMTs located in any of the TPCs.

The scintillation and the ionization signal clusters are matched during the offline data processing. In the matching algorithm, the time of the scintillation cluster is referred as the reference time. The scintillation and ionization clusters belong to the same event of a  $\gamma$ -ray interaction if the time difference between these two clusters is less than the maximum drift time, i.e., the time required for the charge carriers to travel the greatest distance from the cathode to the anode in the LXeTPC. The maximum drift time for the updated XEMIS1 detector corresponds to 28  $\mu\text{s}$ . In the case of the XEMIS2 camera, the maximum drift time for a drift length of 12 cm is about 52  $\mu\text{s}$ .

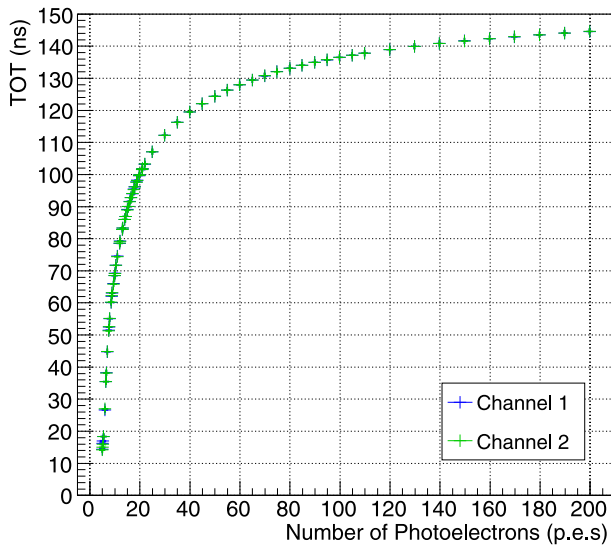


Fig. 3. Time Over Threshold (TOT) conversion curves for PMT channel-1 and PMT channel-2 obtained from calibration corresponding to the threshold level of 88 fC applied in the scintillation signal measurement system of the updated version of the XEMIS1 detector.

### 3.2. Calibration of scintillation signal front-end read-out electronics

The 2-channel prototype electronics of XSRETOT PCB was implemented outside the updated XEMIS1 detector operating at room temperature. The charge can be directly injected into the XSRETOT PCB using a capacitor recharged by a set of square pulses, which serves as a charge injector. The overall performance of the XSRETOT prototype electronics has been characterized and calibrated through the charge injector. The performance results indicate that the PSA has a good linearity response and low electronic noise, presenting quite uniform features for each XSRETOT channel. In the context of a few p.e.s collected by one PMT channel, the time resolution of the signal read-out and DAQ system is predominated by the intrinsic time resolution of LXe scintillation light emission compared to the time jitter of the corrected times using the leading edge correction method for the XSRETOT card (less than 5 ns). A sampling frequency of 100 MHz is adequate for the FPGA in the XDC. Moreover, in the context of few p.e.s collection, the number of collected p.e.s is easily measurable through the TOT method employed in XSRETOT, as presented in Fig. 3.

### 3.3. Calibration of PMT gain

The full XEMIS2 scintillation and ionization signals read-out and DAQ system prototypes were validated in the updated XEMIS1 detector under the XEMIS2 expected operation condition. Two 1-inch square Hamamatsu R7600-06MOD-ASSY PMTs are located at the periphery of the updated XEMIS1 LXeTPC side by side, fully immersed in the LXe. The gain of each PMT has been calibrated employing the XSRETOT prototype electronics. The PMTs are lighted by a very low light intensity HLMP-CB Light Emitting Diode (LED) connected with a 200  $\mu\text{m}$  thick optical fiber that extends to the inside of the LXeTPC [15]. The waveform generator (Agilent 33250A) was connected with the 8-channel 12-bit Analog-to-Digital Converter (ADC) with a 250 MHz sampling frequency for triggering purposes. The gain of each PMT can be measured and monitored during the operation through this PMT calibration setup. The calibration results indicated that the PMT gain increases exponentially with the supply voltage of the PMT, up to the normal operating limit of the PMT (900 V). The PMT gain daily measurements for PMT channel-1 during two months of operation of

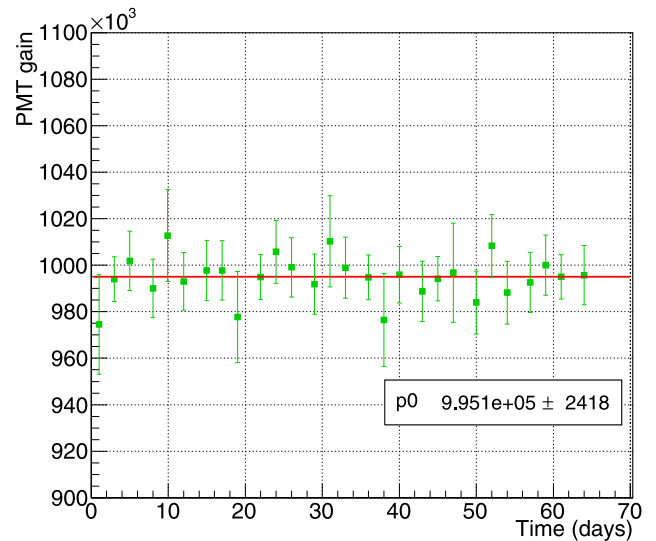


Fig. 4. PMT gain daily measurements for PMT channel-1 during two months of operation of the XEMIS1 experiment.

the XEMIS1 experiment are presented in Fig. 4. The gain of PMT is nearly stable during the detector operation at steady conditions (1.2 bar and 168 K). High voltages will be adjusted to reach the same gain for all PMTs in XEMIS2.

### 3.4. Virtual segmentation of XEMIS1 detector with light collection map

To enhance the administered activity to 200 kBq, it is possible to delimit a virtual volume by determining the detection zone of each PMT in the LXeTPC, which can be used in the spatial pre-localization of the physical events to decrease the occupancy rate of the LXeTPC. Specifically, the Light Collection Map (LCM) presents the average number of p.e.s collected by each PMT in relation to the source position. The LCMs were obtained to carry out the virtual fiducialization of the active volume of the LXeTPC.

In our experiment, a ( $\beta^+$ ,  $\gamma$ ) radionuclide sodium-22 ( $^{22}\text{Na}$ ) with an activity of 3.3 kBq, which emits a positron and a 1.274 MeV  $\gamma$ -ray in quasi-coincidence, is used to characterize the updated XEMIS1 detector. The experimental LCMs of XEMIS1 active volume were established from the experimental data by selecting specifically the photoelectric events of 511 keV  $\gamma$ -ray that deposit all the energy inside the active volume of the LXeTPC after one interaction despite the small size of the updated XEMIS1 detector. The experimental LCMs of the average number of p.e.s collected by both PMT channels in the updated XEMIS1 detector are shown in Figs. 5 and 6. In each figure, the small images from the top left to the bottom right represent in sequence the LCM slices on the z-axis from the anode to the cathode. Each pixel in the small image corresponds to the average number of detected p.e.s emitted from the 511 keV photoelectric events whose interaction positions are in a  $2 \times 2 \times 2 \text{ mm}^3$  cube.

The experimental LCMs indicate that each PMT owns an individual FOV. In addition, when the interaction positions of the photoelectric effect (i.e., the scintillation light emission positions) are opposite to the PMT entrance window, the maximum number of p.e.s are detected. Besides, almost no dead zone for light collection is found in the XEMIS1 active region.

## 4. Conclusion

The preparation work for the XEMIS2 camera operation has been carried out in an updated version of the XEMIS1 detector. The cost-effective self-triggering scintillation signal read-out and DAQ system

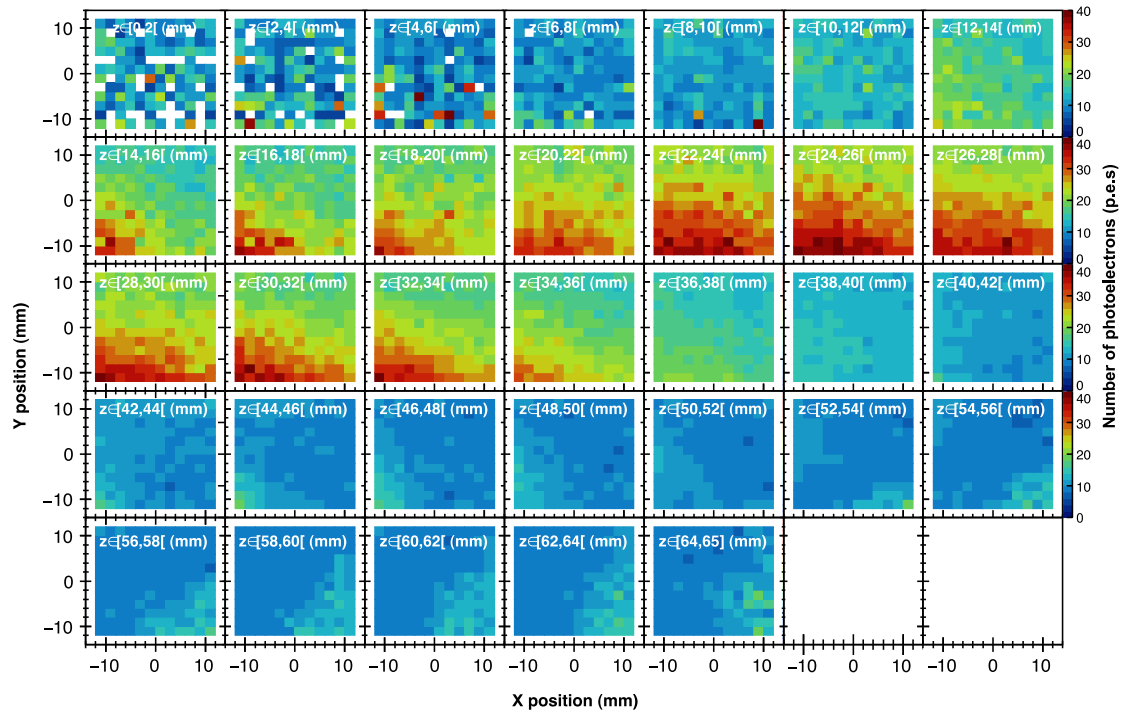


Fig. 5. Experimental light collection map of the average number of photoelectrons collected by PMT channel-1 for 511 keV deposited energy in the updated version of the XEMIS1 detector.

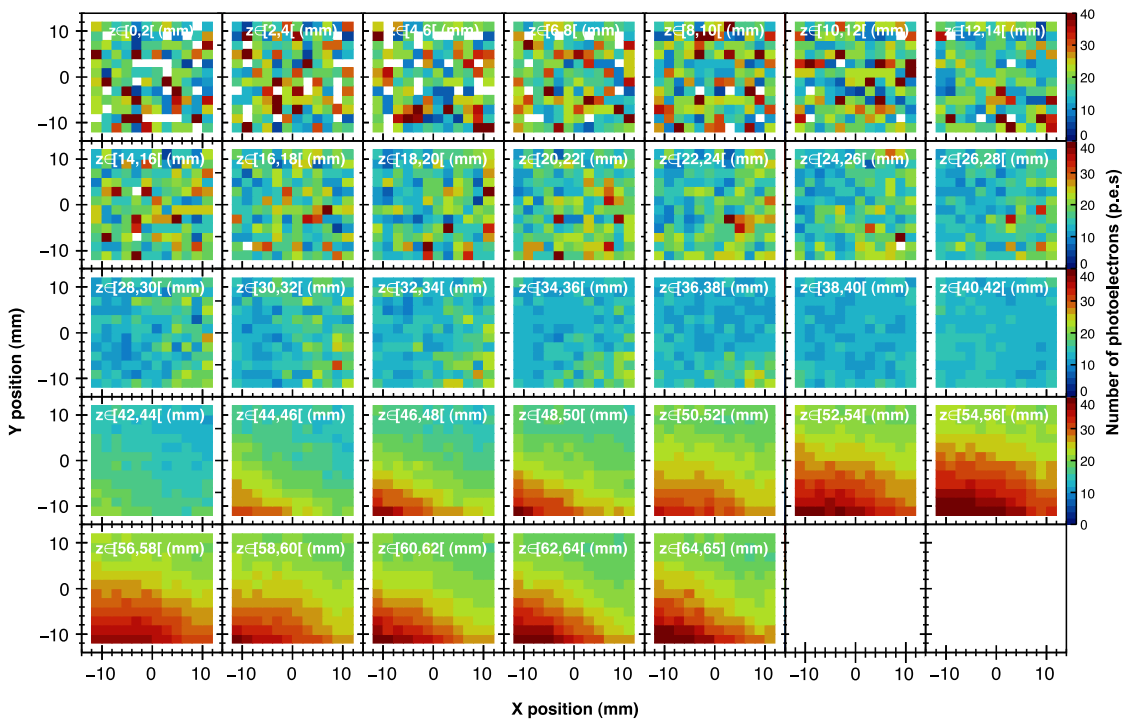


Fig. 6. Experimental light collection map of the average number of photoelectrons collected by PMT channel-2 for 511 keV deposited energy in the updated version of the XEMIS1 detector.

has been developed for the XEMIS2 camera to extract the  $\gamma$ -ray interaction time and the approximate number of detected p.e.s from the scintillation signals. This DAQ prototype has been installed and qualified in XEMIS1: its results indicate good performance in scintillation light measurement. Moreover, the experimental LCMs of XEMIS1 LXeTPC have been built: they can be used for the optimization of

the matching algorithm of scintillation and ionization signals, and the virtual segmentation of the active zone. This spatial pre-localization of the physical events is used for lowering the detector occupancy rate under the circumstance of increasing the administered activity to lessen the examination time. The XEMIS2 camera was moved and installed in the “Centre d’Imagerie Multi-modalités et Applications”

(CIMA) at Nantes CHU. The commissioning of the XEMIS2 scintillation light measurement system is undergoing in CIMA.

### Declaration of competing interest

The authors declare that they have no known competing financial interests or personal relationships that could have appeared to influence the work reported in this paper.

### Acknowledgments

The research presented in this paper has been funded by the E.U., the Region Pays de la Loire in France, and by grants from the French National Research Agency, “Investissement d’Avenir” Arronax-Plus Equipex no ANR-11-EQPX-0004.

### References

- [1] C. Grignon, et al., Nuclear medical imaging using  $\beta + \gamma$  coincidences from  $^{44}\text{Sc}$  radio-nuclide with liquid xenon as detection medium, *Nucl. Instrum. Methods A* 571 (2007) 142–145.
- [2] S. Huclier-Markai, et al., Promising Scandium Radionuclides for Nuclear Medicine: A Review on the Production and Chemistry up to *In Vivo* Proofs of Concept, *Cancer Biother. Radiopharm.* 33 (2018) 316–329.
- [3] D. Giovagnoli, et al., A Pseudo-TOF Image Reconstruction Approach for Three-Gamma Small Animal Imaging, *IEEE Trans. Rad. Plasma Med. Sci.* 5 (2021) 826–834.
- [4] L. Gallego Manzano, et al., XEMIS: A liquid xenon detector for medical imaging, *Nucl. Instrum. Methods A* 787 (2015) 89–93.
- [5] Y. Xing, et al., XEMIS: Liquid Xenon Compton Camera for  $3\gamma$  Imaging, *Springer Proc. Phys.* 213 (2017) 154–158, [http://dx.doi.org/10.1007/978-981-13-1316-5\\_29](http://dx.doi.org/10.1007/978-981-13-1316-5_29).
- [6] L. Gallego Manzano, et al., XEMIS2: A liquid xenon detector for small animal medical imaging, *Nucl. Instrum. Methods A* 912 (2018) 329–332.
- [7] Y. Xing, et al., Direct Measurement of Ionization Charges in Single-phase Liquid Xenon Compton Telescope for  $3\gamma$  Medical Imaging, in: 2019 IEEE Nuclear Science Symposium and Medical Imaging Conference, NSS/MIC, 2019, pp. 1–4, <http://dx.doi.org/10.1109/NSS/MIC42101.2019.9059808>.
- [8] L. Virone, et al., Gravity assisted recovery of liquid xenon at large mass flow rates, *Nucl. Instrum. Methods A* 893 (2018) 10–14.
- [9] J.P. Cussonneau, et al.,  $3\gamma$  Medical Imaging with a Liquid Xenon Compton Camera and  $^{44}\text{Sc}$  Radionuclide, *Acta Phys. Polon. B* 48 (2017) 1661–1667, <http://dx.doi.org/10.5506/APhysPolB.48.1661>.
- [10] E. Aprile, et al., Simultaneous Measurement of Ionization and Scintillation from Nuclear Recoils in Liquid Xenon for a Dark Matter Experiment, *Phys. Rev. Lett.* 97 (2006) 081302.
- [11] T. Doke, Fundamental properties of liquid argon, krypton and xenon as radiation detector media, *Portugal. Phys.* 12 (1981) 9–48.
- [12] S. Kubota, M. Hishida, M. Suzuki, J.Z. Ruan, Dynamical behavior of free electrons in the recombination process in liquid argon, krypton, and xenon, *Phys. Rev. B.* 20 (1979) 3486–3496, <http://dx.doi.org/10.1103/PhysRevB.20.3486>.
- [13] Y. Zhu, et al., XEMIS2: A liquid xenon Compton camera to image small animals, in: 2019 IEEE 20th International Conference on Dielectric Liquids, ICDL, 2019, pp. 1–4, <http://dx.doi.org/10.1109/ICDL.2019.8796534>.
- [14] G.F. Knoll, *Radiation Detection and Measurement*, fourth ed., John Wiley & Sons, 2010.
- [15] Y. Zhu, et al., XEMIS2 Liquid Xenon Compton Camera for Small Animal  $3\gamma$  Medical Imaging: Scintillation Light Measurement, in: 2019 IEEE Nuclear Science Symposium and Medical Imaging Conference, NSS/MIC, 2019, pp. 1–4, <http://dx.doi.org/10.1109/NSS/MIC42101.2019.9059638>.